Surface mode enhancement of the Goos-Hänchen shift in direct reflection off antiferromagnets

V. B. Silva and T. Dumelow*

Departamento de Física, Universidade do Estado do Rio Grande do Norte, Costa e Silva, 59625-620 Mossoró RN, Brazil

(Received 1 March 2018; published 29 June 2018)

We examine how, in the presence of an external magnetic field, the Goos-Hänchen shift for terahertz radiation reflected, at oblique incidence, off an antiferromagnet can show significantly enhanced values under the right circumstances. Such enhanced shifts, which have associated absorptions in the presence of damping, occur in one of the magnon reststrahl regions and are related to the excitation of surface resonances, which can be considered as extensions of surface polariton modes into the reflectivity regime. Although the enhancement of the Goos-Hänchen shift due to surface modes is well known in the attenuated total reflection configuration using a three-layer prism geometry, such effects have not previously been reported in direct reflection and only occur here due to the presence of the externally applied field. We confirm the effect using simulations for reflection off MnF_2 at low temperature and show that only a small applied field is necessary to induce a significant enhancement along with an associated sharp absorption. For a larger field, the effects are less distinct.

DOI: 10.1103/PhysRevB.97.235158

I. INTRODUCTION

In conventional optics, a finite beam reflected from a plane surface is considered to reflect from the point at which the incident beam strikes the surface. In many situations, however, the reflected beam can undergo a lateral shift, known as the Goos-Hänchen shift, along the surface. Original studies concentrated on such a shift in total internal reflection [1], but recent works have shown examples where the phenomenon may occur on external reflection from air or vacuum if there are evanescent fields in the second medium [2–5].

There are several ways of interpreting such shifts. We particularly note the plane wave interference (angular spectrum) model [6–8] and the energy conservation model [9–11]. In the first approach, the incident beam is considered to be made up of a series of plane waves, each with a slightly different incident angle. If the interference between the plane waves of the reflected beam is slightly different from that of the incident beam, this can appear as a lateral shift of the reflected beam. The second approach interprets the shift as arising from energy flow along the surface associated with the evanescent fields in the second medium.

Several studies have shown how surface polaritons can enhance the Goos-Hänchen shift [12–17]. True surface polaritons are characterized by exponential field decay on either side of the interface. Since the incident beam in a reflection experiment is, by definition, propagating, one cannot normally excite such polaritons in direct reflection, so a two-layer geometry is not sufficient. Thus a multilayer system is usually necessary, typically an attenuated total reflection setup in which the incident layer is a prism, the incident angle within the prism being greater than the critical angle for total internal reflection.

In this paper we show how, on reflection from the right type of medium, there can be an enhanced shift related to surface polaritons even in simple reflection from a semi-infinite crystal. The crystal considered here is an antiferromagnet, and the experiment is to be conducted in the presence of an external field.

It has already been demonstrated that Goos-Hänchen shifts on reflection off magnetic media of this type can display a number of unusual properties [18–22]. The shifts, which occur in the region of the magnon resonance frequencies, are typically tunable using an externally applied field. They may be nonreciprocal and even occur at normal incidence [18,19]. In the case of the simulations of direct reflection off MnF_2 presented by Macêdo *et al.* [21], the shifts appear to be enhanced at certain frequencies, as pointed out by Savchenko *et al.* [23], who considered such enhancements in the case of zero absorption. In the present paper we show that these enhancements can be regarded as due to surface resonances, directly related to surface polariton modes. We use a different geometry from that studied by Macêdo *et al.*, however, as much smaller fields are required to achieve the same effect.

The structure of the paper is as follows. In Sec. II we present the basic methodology used in calculating the reflectivity and Goos-Hänchen shift. In Sec. III we present results in the absence of absorption and use a simple power flow model to show the condition for the enhanced shift. In Sec. IV we include damping effects and calculate surface resonance frequencies. The enhanced shifts are seen to occur at such frequencies, at which there are also sharp absorption dips. These phenomena are used to give a better physical description of the modes. Finally, in Sec. V, we summarize the results and present concluding remarks.

II. BASIC DISLOCATION CALCULATION

The calculation of the Goos-Hänchen shift, using the angular spectrum approach, in oblique incidence reflection off an antiferromagnet in the Voigt geometry has previously

*Corresponding author: tdumelow@yahoo.com.br

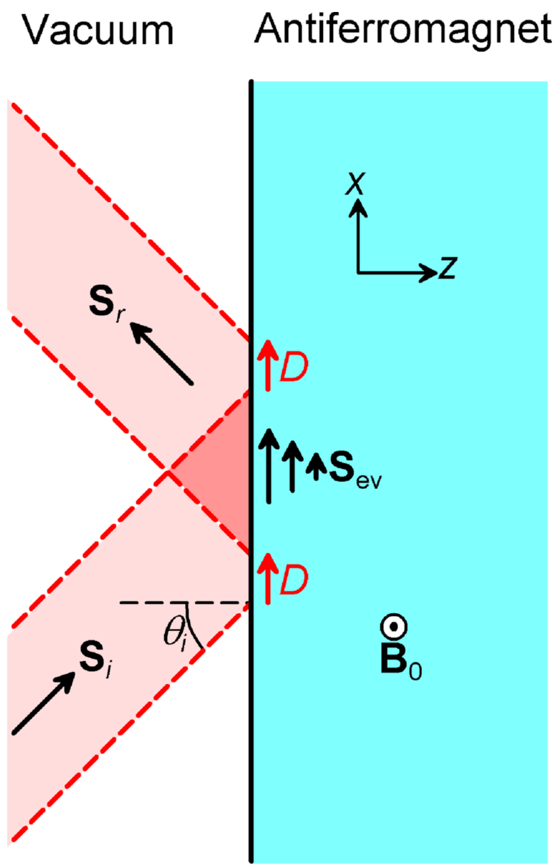

FIG. 1. Geometry considered in this paper for reflection of a finite beam off an antiferromagnet.

been presented by Lima *et al.* [20]. Here we summarize the procedure.

We consider reflection from a semi-infinite antiferromagnet in the geometry shown in Fig. 1. A finite beam is incident from vacuum at an angle θ_i in s polarization (**E**-field perpendicular to the plane of incidence). The antiferromagnet easy axis is along y, perpendicular to the plane of incidence, as is the applied field $\mathbf{B}_0$. D represents the lateral displacement of the reflected beam along x.

At frequency ω, the antiferromagnet permeability tensor in this geometry is of the form [24]

$$\mu = \begin{pmatrix} \mu_1 & 0 & i\mu_2 \\ 0 & 1 & 0 \\ -i\mu_2 & 0 & \mu_1 \end{pmatrix}, \tag{1}$$

where

$$\mu_1 = 1 + \mu_0\gamma^2 B_A M_S(Y^+ + Y^-), \tag{2a}$$

$$\mu_2 = \mu_0\gamma^2 B_A M_S(Y^+ - Y^-), \tag{2b}$$

$$Y^\pm = \left[\omega_r^2 - (\omega \pm \gamma B_0 + i\Gamma)^2\right]^{-1}. \tag{2c}$$

Here B_A is the anisotropy field, M_S the sublattice magnetization, γ the gyromagnetic ratio, Γ the damping parameter, and ω_r the zero-field magnetic resonance frequency given by

$$\omega_r = \gamma\left(2B_A B_E + B_A^2\right)^{1/2}, \tag{3}$$

where B_E is the exchange field. In the absence of an externally applied field ($B_0 = 0$), the tensor is diagonal ($\mu_2 = 0$), but the antiferromagnet becomes gyromagnetic ($\mu_2 \neq 0$) if B_0 is nonzero, leading to nonreciprocal effects.

In the geometry of Fig. 1, the s-polarized reflection coefficient, i.e., the complex ratio between the E_y fields of the reflected and incident beams, is given by [25]

$$r = \frac{k_{1z}\mu_v - k_{2z} - ik_x(\mu_2/\mu_1)}{k_{1z}\mu_v + k_{2z} + ik_x(\mu_2/\mu_1)}. \tag{4}$$

Here, μ_v is the Voigt permeability, given by

$$\mu_v = \frac{\mu_1^2 - \mu_2^2}{\mu_1}, \tag{5}$$

and k_x, k_{1z}, and k_{2z} are the wave-vector components in the two layers. The in-plane component k_x is the same in both media and is given by

$$k_x = k_0 \sin\theta_i, \tag{6}$$

where $k_0 = \omega/c$, and the z components in layer 1 (vacuum) and layer 2 (antiferromagnet) are given by [25]

$$k_{1z} = \left(k_0^2 - k_x^2\right)^{1/2}, \tag{7a}$$

$$k_{2z} = \left(\epsilon\mu_v k_0^2 - k_x^2\right)^{1/2}, \tag{7b}$$

respectively, where ϵ is the dielectric constant of the antiferromagnet. The reflection coefficient of Eq. (4) can be expressed in terms of an amplitude ρ and a phase ϕ,

$$r = \rho\exp(i\phi), \tag{8}$$

with the power reflectivity R equal to ρ^2.

The above results are strictly speaking true for plane waves. However, we can consider a finite beam as a Fourier sum of plane waves. Thus, ignoring time dependence, the incident beam can be represented as

$$E_i(x,z) = \int_{-k_0}^{k_0} \psi(k_x)\exp[i(k_x x + k_{1z}z)]dk_x, \tag{9}$$

where k_x is the in-plane component of the associated wave vector and $\psi(k_x)$ is a distribution function representing the shape of the beam.

Assuming the reflected phase is dependent on k_x, the interference between the plane wave components for the reflected beam will be different from that of the incident beam. McGuirk and Carniglia [8] have shown that, provided that the distribution of k_x values is sufficiently narrow (i.e., the beam is sufficiently wide), the resulting beam profile is the same as that of the incident beam but displaced along x by a distance

$$D = -\left.\frac{d\phi}{dk_x}\right|_{k_x = k_{x0}}, \tag{10}$$

where k_{x0} is the k_x value at the center of the distribution, i.e., the k_x value obtained from Eq. (6) for the overall beam.

III. BEAM REFLECTION IN THE ABSENCE OF ABSORPTION

We start by considering reflection and beam shifts in the absence of absorption, equivalent to putting $\Gamma = 0$ in Eq. (2c),

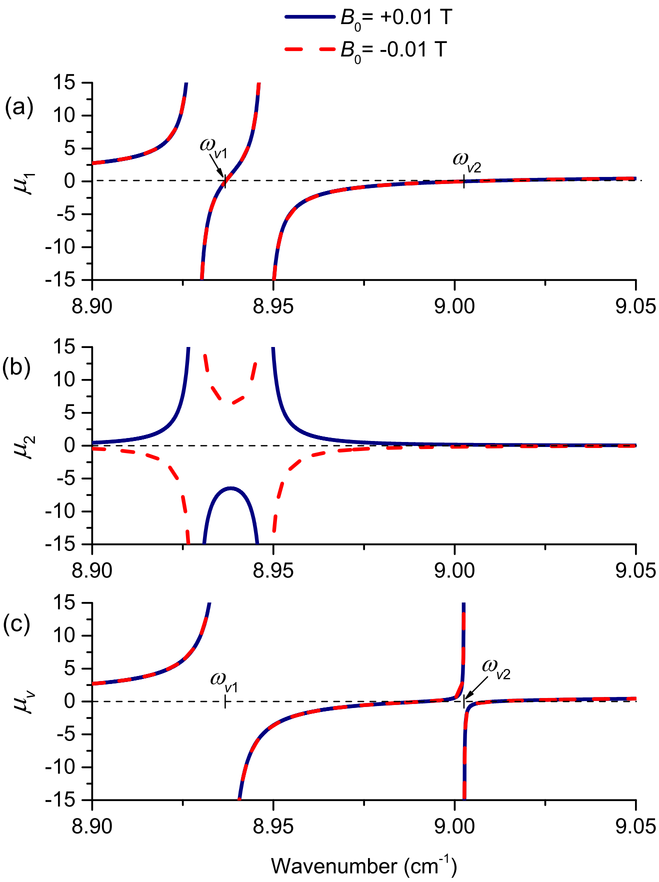

FIG. 2. (a) μ_1, (b) μ_2, and (c) μ_v plotted against wave number $\omega/2\pi c$ for MnF_2 in an external field B_0 of $+0.01$ T (solid blue lines) and -0.01 T (dashed red lines), ignoring damping.

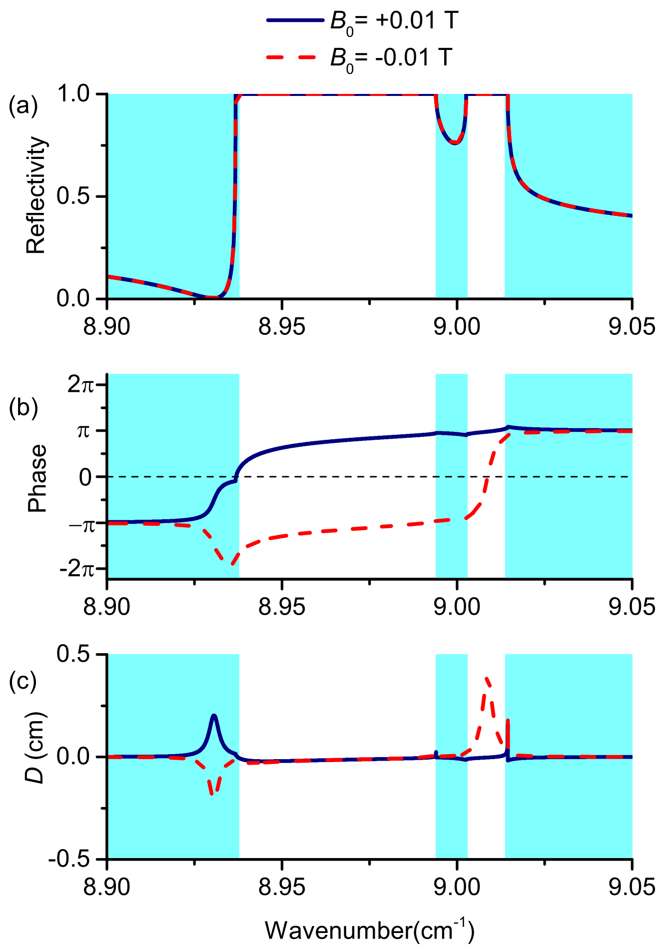

FIG. 3. Calculated (a) reflectivity, (b) phase, and (c) Goos-Hänchen shift for reflection off MnF_2 at an incident angle of 45° in an external field B_0 of $+0.01$ T (solid blue lines) and -0.01 T (dashed red lines), ignoring damping. The shaded regions represent the bulk regions, in which k_{2z} is real. The phase is represented in part (b) as extending outside the range $-\pi \leqslant \phi \leqslant \pi$ in order to show its variation as continuous curves.

in the case of reflection off an antiferromagnet, and consider the condition for advanced shifts. The antiferromagnet considered here is MnF_2 at 4.2 K. The material parameters used are [26]: $M_S = 6.0 \times 10^5$ A/m, $B_A = 0.787$ T, $B_E = 53.0$ T, and $\gamma/2\pi c = 0.975$ cm^{-1}/T, corresponding to $\omega_r/2\pi c = 8.94$ cm^{-1}, with a dielectric constant ϵ equal to 5.5.

We consider an applied field B_0 of ± 0.01 T, leading to μ_1 and μ_2 values shown in Figs. 2(a) and 2(b), respectively, where they are plotted against frequency expressed in wave-number units $\omega/2\pi c$. The nonzero field leads to two resonances, with the sign of B_0 reversing the sign of μ_2. In order to interpret the reflectivity behavior, it is often more useful to consider the Voigt permeability μ_v, given by Eq. (5), than the components μ_1 and μ_2 individually. This is shown in Fig. 2(c) and is independent of the sign of B_0. It is seen once again that there are two resonances but now the resonance frequencies, marked as ω_{v1} and ω_{v2}, are at the zeros in μ_1 rather than at the poles.

At normal incidence, the regions of negative μ_v correspond to imaginary k_{2z} [see Eq. (7b)] and hence total reflection ($R = 1$). For convenience, we refer to such total reflection regions as reststrahl regions, as opposed to bulk regions in which k_{2z} is real and $R < 1$. Our main interest here is in the upper reststrahl region, whose lower limit is ω_{v2}, with an upper limit that increases with incident angle [see Eq. (7b)]. The value of μ_1 in this reststrahl is always small and positive.

The resulting reflectivity for an incident angle of 45° is shown in Fig. 3(a), and the two reststrahl regions are clearly seen. The reflectivity is also seen to be reciprocal, i.e., $R(B_0) = R(-B_0)$. Reciprocal reflectivity in the absence of absorption is a well-known result [27] and has been demonstrated using thermodynamic arguments [28]. The reflected phase ϕ, on the other hand, is distinctly nonreciprocal [29], as seen in Fig. 3(b). This nonreciprocity can be considered as the source of a nonreciprocal Goos-Hänchen shift as represented by Eq. (10) [20], and such nonreciprocity is seen in the shifts calculated using this equation in Fig. 3(c).

Within the upper reststrahl region the phase passes through zero when the applied field is negative but not when it is positive. This can be seen from Eq. (4) when one notes that, in the reststrahl region, the first term in both the numerator and denominator is real, while the second and third terms are imaginary. Thus the $\phi = 0$ condition, which turns out to have particular relevance in terms of enhancement of the Goos-Hänchen shift, corresponds to

$$k_{2z} + ik_x\frac{\mu_2}{\mu_1} = 0 \tag{11}$$

so that, for k_x positive, μ_1 and μ_2 must have opposite signs, corresponding, in the upper reststrahl region, to negative B_0 (see Fig. 2). Indeed, the phenomenon of the reflected phase passing through zero does not occur in reststrahl regions in conventional reflection setups in the absence of an external magnetic field.

Substitution of the k_{2z} value from Eq. (7b) into Eq. (11) leads to the simple relation

$$k_x^2 = k_0^2 \epsilon \mu_1 \tag{12}$$

for $\phi = 0$. A similar equation was also obtained by Savchenko *et al.* [23] for the antiferromagnet easy axis along x.

The frequency at which the phase passes through zero is of particular significance because, as seen in Fig. 3(c), there is a substantial enhancement in the Goos-Hänchen shift at this frequency. A crude energy flow model of the type proposed by Renard [9] shows how a shift maximum should be expected when this condition is met. Basically, one considers beam reflection at the interface in terms of three regions along x, as shown in Fig. 1. Behavior in the central region can be considered in terms of total plane wave reflection. Within the antiferromagnet, in this region, there is energy flow along x within an evanescent wave. Due to energy conservation, there must be a region at one edge of the beam in which power is entering from vacuum to the antiferromagnet and another at the other edge of the beam where it leaves, leading to a shift D of the beam (see Fig. 1). Assuming power flow restricted to the xz plane, we then get

$$\langle S_i \rangle D \cos\theta_i = \int_0^\infty \langle S_{\mathrm{ev}} \rangle dz, \tag{13}$$

where $\langle S_i \rangle$ and $\langle S_{\mathrm{ev}} \rangle$ are the magnitudes of the time-averaged Poynting vectors of the incident wave in vacuum and of the evanescent wave within the antiferromagnet, respectively.

Thus it is clear that maximizing the right hand side of Eq. (13) will maximize the displacement D. We therefore look at $\langle S_{\mathrm{ev}} \rangle$ at the interface when $\phi = 0$ to see how this maximization takes place. We consider an incident plane wave with electric field

$$\mathbf{E}_i = E_0 \exp[i(k_x x + k_{1z} z - \omega t)]\hat{\mathbf{a}}_y \tag{14}$$

and magnetic field

$$\mathbf{H}_i = H_0 \exp[i(k_x x + k_{1z} z - \omega t)](-\cos\theta_i \hat{\mathbf{a}}_x + \sin\theta_i \hat{\mathbf{a}}_z), \tag{15}$$

where E_0 and H_0 are considered real, with $\langle S_i \rangle = (1/2)E_0 H_0$.

Since, in the present case, phase is defined by comparing incident and reflected E_y fields at the interface, and reflection is total, the incident and reflected E_y components are equal when $\phi = 0$, interfering constructively to give an overall E_y field equal to $2E_{iy}$ at the surface. In a similar way, the incident and reflected H_x components cancel each other at the surface, and the incident and reflected H_z field components interfere constructively leading to an overall H_z field of $2H_{iz}$. The absolute values of the complex amplitudes $|E_y|$ and $|H_z|$ therefore reach maximum values at the interface, equal to $2E_0$ and $2H_0 \sin\theta_i$, respectively, with $|H_x| = 0$. This is seen in Figs. 4(a)–4(c) which show the limits $\pm|E_y|$, $\pm|H_x|$, and $\pm|H_z|$ of the various field components as a function of z for $B_0 = +0.01$ T and

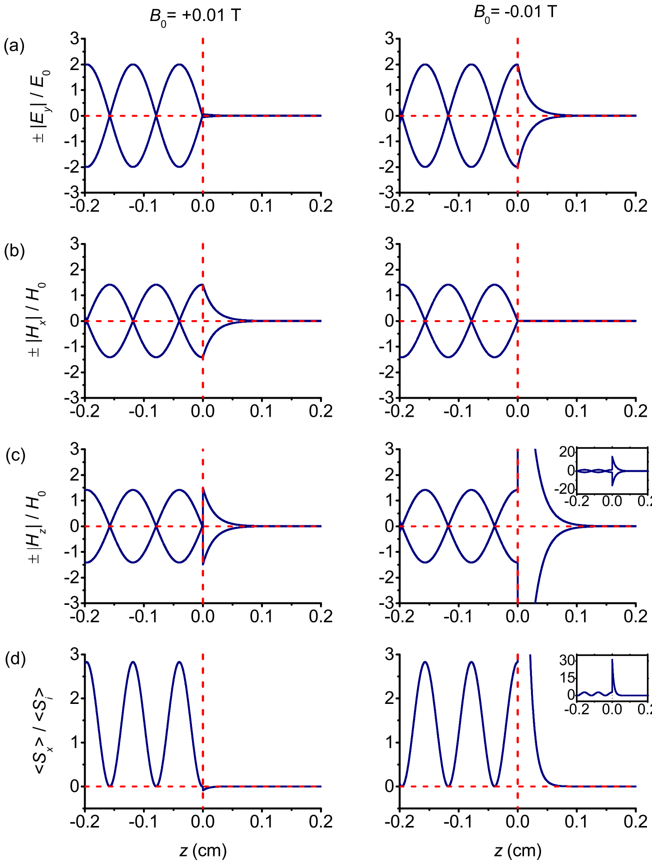

FIG. 4. Limits of the (a) E_y field, (b) H_x field, and (c) H_z field with position z, normalized to incident wave values, for an s-polarized plane wave reflected off the surface of an antiferromagnet, with $\theta_i = 45^\circ$, in an external field B_0 of $+0.01$ T (left hand figures) and -0.01 T (right hand figures). (d) Time averaged Poynting vector along z compared to $\langle S_i \rangle$. Calculations were performed at a frequency corresponding to a wave number of 9.0087 cm^{-1}, at which $\phi = 0$ for $B_0 = -0.01$ T. The insets in parts (c) and (d) of the $B_0 = -0.01$ T graphs show the results on a reduced vertical scale to indicate the full range of the values when $x > 0$.

$B_0 = -0.01$ T at the relevant frequency, displaying a standing wave pattern within the incident (vacuum) layer, corresponding to $z < 0$. In the $B_0 = -0.01$ T case, for which $\phi = 0$, there are thus antinodes in E_y and H_z and a node in H_x at the interface. For $B_0 = +0.01$ T, however, the phase ϕ is nearly π, and there are nodes in E_y and H_z and an antinode in H_x close to the interface.

Continuity across the interface means that the enhanced E_y and H_z values in vacuum in the $B_0 = -0.01$ T case lead to enhanced E_y and H_z fields in the antiferromagnet. The absolute amplitudes of the fields in the antiferromagnet ($z > 0$) then become

$$|E_y| = 2E_0 \exp(ik_{2z} z) \tag{16a}$$

$$|H_x| = 0 \tag{16b}$$

$$|H_z| = \frac{2H_0 \sin\theta_i}{\mu_1} \exp(ik_{2z} z), \tag{16c}$$

where μ_1 is a small positive quantity (0.017 at the frequency considered) and k_{2z} is imaginary, leading to evanescent decay along z. Both E_y and H_z are in phase with each other, so there is an enhanced average power flow $\langle S_x \rangle$, equal to $(1/2)|E_y||H_z|$, along x in the antiferromagnet for $B_0 = -0.01$ T compared with a negligible power flow for $B_0 = +0.01$ T, as confirmed by Fig. 4(d). In addition, since H_x is always zero at the interface, there is no power flow across the interface.

The power flow S_x in the figure, in the case of $z > 0$, is the same as S_{ev} in Eq. (13), so it is straightforward to apply the above $\phi = 0$ results with this equation to obtain the Goos-Hänchen shift D. The result is

$$D = -\frac{2 \tan \theta_i}{k_0 \mu_2 \sqrt{\epsilon \mu_1}}. \tag{17}$$

It is worth noting that this result is in exact agreement with that obtained using the plane wave interference model, as represented by Eq. (10), when $\phi = 0$. Agreement between the two models only occurs in exceptional circumstances due to interference in the incident medium associated with instantaneous power flow across the interface, which is not accounted for in the Renard model [10]. In the present case, however, S_z is always zero at the interface, and there are no such interference effects.

In Fig. 5 we show reflection, phase, and Goos-Hänchen shift as a function of both frequency and in-plane wave vector k_x for both $B_0 = +0.01$ T and $B_0 = -0.01$ T, with reflection taking place for $|k_x| < k_0$ ($\theta_i < 90°$). Figure 5(a) shows how the width of the reststrahl regions increases with incident angle (or k_x) and confirms that reflectivity is reciprocal for all angles of incidence. Figure 5(b) shows the reflected phase ϕ, and it is seen that, in the case of $B_0 = -0.01$ T, the phase always passes rapidly through zero in the upper reststrahl region, thus appearing as a narrow white line in the figure. This does not occur in the $B_0 = +0.01$ T figure. Figure 5(c) shows the Goos-Hänchen shift, which peaks along the $\phi = 0$ line of Fig. 5(b) for $B_0 = -0.01$ T. This is confirmed by the crosses on the plot which represent the solution of $\phi = 0$ as a function of k_x. Such solutions do not exist for $B_0 = +0.01$ T. Thus it is confirmed that, in a model that ignores absorption, enhanced Goos-Hänchen shifts should occur when the reflected phase passes through zero in a reststrahl region, and it is reasonable to expect this behavior to persist when absorption is incorporated.

IV. RELATION OF THE ENHANCED GOOS-HÄNCHEN SHIFT TO SURFACE MODES

In this section we examine how the enhanced Goos-Hänchen shifts discussed in the previous section can be interpreted in terms of a type of electromagnetic surface resonance, based on surface polariton modes. Surface polaritons are characterized by exponential field decay either side of an interface. In the case of an antiferromagnet/vacuum interface in the geometry considered here, such modes have a dispersion relation [30]

$$k_{1z} + \frac{k_{2z}}{\mu_v} + i\frac{k_x \mu_2}{\mu_v \mu_1} = 0, \tag{18}$$

equivalent to putting the denominator of Eq. (4) equal to zero.

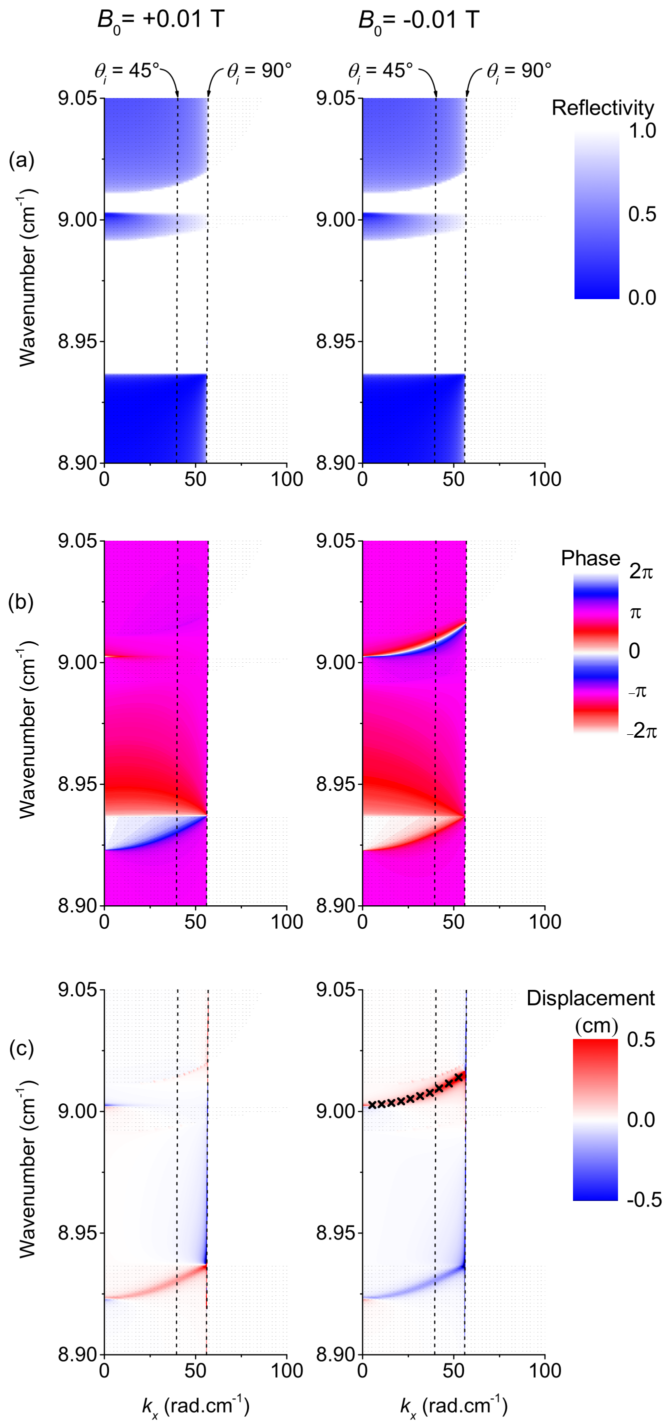

FIG. 5. Calculated (a) reflectivity, (b) phase, and (c) Goos-Hänchen shift for reflection off MnF_2 as a function of both wave number and k_x in an external field B_0 of +0.01 T (left hand figures) and −0.01 T (right hand figures), ignoring damping. The crosses in part (c) represent the frequencies for which $\phi = 0$. The dotted regions represent the bulk regions, in which k_{2z} is real.

In the absence of damping effects, the third term is imaginary, so both k_{1z} and k_{2z} should also be imaginary for Eq. (18) to be satisfied. For simple reflection, the largest possible value of k_x is k_0, corresponding to $\theta_i = 90°$. For $|k_x| < k_0$, k_{2z} is real in the bulk regions and imaginary in the reststrahl regions,

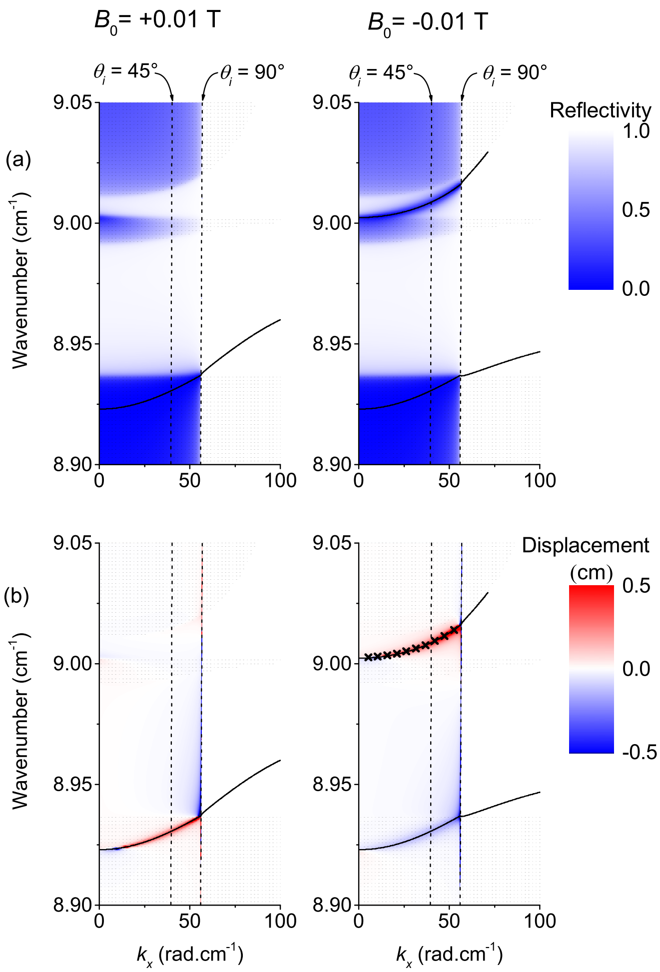

FIG. 6. Calculated (a) reflectivity and (b) Goos-Hänchen shift for reflection off MnF_2 as a function of both wave number and k_x in an external field B_0 of +0.01 T (left hand figures) and −0.01 T (right hand figures), taking damping into account. The solid lines represent surface resonance dispersion curves $\mathrm{Re}(\omega/2\pi c)$ vs k_x. The crosses in part (b) represent the frequencies for which $\phi = 0$ in the absence of damping. The dotted regions represent the bulk regions, in which k_{2z} is real without damping.

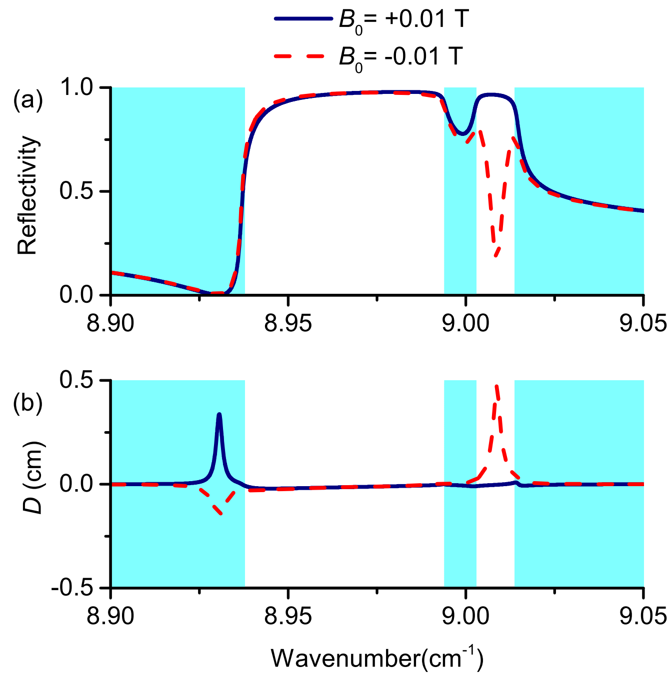

FIG. 7. Calculated (a) reflectivity and (b) Goos-Hänchen shift for reflection off MnF_2 at an incident angle of 45° in an external field B_0 of +0.01 T (solid blue lines) and −0.01 T (dashed red lines), taking damping into account. The shaded regions represent the bulk regions, in which k_{2z} is real, ignoring damping.

whereas k_{1z} is always real. Therefore surface polaritons are only considered as being excited for $|k_x| > k_0$. In the various diagrams of Fig. 6 the solid curves in the region to the right of the line marked $\theta_i = 90^\circ$ represent such modes. There are surface polariton modes associated with the lower reststrahl region for both positive and negative applied magnetic fields, although the two curves are different, indicating nonreciprocal behavior. With regard to the upper reststrahl region, however, there is only a surface polariton mode when the applied field is negative.

Even though strict surface polariton modes are not possible for $|k_x| < k_0$, it is still possible to obtain solutions, often referred to as surface resonances, to Eq. (18) if we let either ω or k_x take complex values, thus allowing exponential decay in both media, and in this case damping effects can be included [31]. Thus, if we take ω to be complex, an experimental frequency scan can be considered as scanning $\mathrm{Re}(\omega)$, with some degree of coupling to modes in the complex frequency plane. Extensions of the surface polariton dispersion curves into the region $k_x < k_0$ calculated in this way are shown in Fig. 6 using a damping parameter [32] of $\Gamma/2\pi c = 0.0007\ \mathrm{cm}^{-1}$ (in practice, the whole curves, including the surface polariton region $k_x > k_0$, were calculated using this method). Figure 6(a) also shows the variation of the reflectivity with k_x and frequency when this damping parameter is included in the calculations, and it is seen that, in this case, the reflectivity shows minima at the surface resonance frequencies. The reflectivity thus shows a nonreciprocity related to the surface resonances.

In principle, the effect of surface resonances on the reflectivity can be seen both in the bulk regions below the lower reststrahl region and within the upper reststrahl region. Nonreciprocal reflection associated with surface resonances in, or at the edge of, the bulk regions has been studied both theoretically and experimentally [31–34]. Nonreciprocal reflection associated with surface resonances within the reststrahl regions, however, has been effectively ignored, although Jensen *et al.* [34] do show a dispersion curve for this type of mode. In the geometry considered here, such effects are not usually observed at higher fields (although nonreciprocal effects in the bulk regions become considerably more pronounced). In the present case, however, Fig. 6(a) shows a distinct dip in reflectivity that accurately follows the surface resonance dispersion curve for $B_0 = -0.01$ T, although there is negligible nonreciprocity in the bulk regions. The resulting reflectivity spectra, for both $B_0 = +0.01$ T and $B_0 = -0.01$ T, are shown in Fig. 7(a) for $\theta_i = 45^\circ$, confirming this result.

It should be mentioned here that the sign of the imaginary component of k_{1z} corresponding to the solution of Eq. (18) is not necessarily positive, as one would expect for exponential

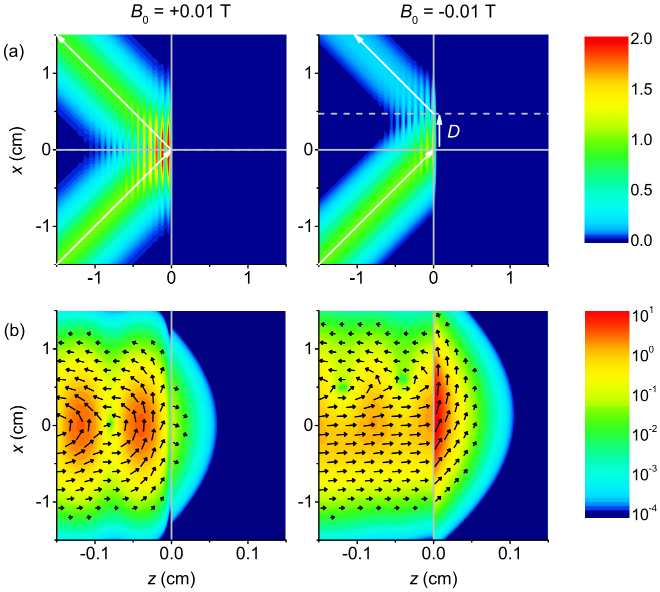

FIG. 8. (a) Reflection of a Gaussian beam, of width $g = 0.5$ cm and an incident angle of 45°, off MnF_2 in the presence of external fields B_0 of $+0.01$ T and -0.01 T at a frequency corresponding to a wave number of $9.0087\ \mathrm{cm}^{-1}$. The horizontal dashed line in the $B_0 = -0.01$ T figure shows the value of D calculated using Eq. (10). (b) Details of power flow near the interface using an expanded horizontal scale. In part (a) the color scale represents power flow intensity on a linear scale, whereas in part (b) both the color scale and the length of the arrows represent power flow intensity on a logarithmic scale.

decay away from the interface. For $\Gamma/2\pi c = 0.0007\ \mathrm{cm}^{-1}$, $\mathrm{Im}(k_{1z})$ is positive for $k_x < 12\ \mathrm{cm}^{-1}$ but is negative for $k_x > 12\ \mathrm{cm}^{-1}$. This imaginary component is always very small, however, and it becomes positive over the whole k_x range up to $k_x = k_0$ if the damping parameter Γ is increased. Despite the apparent discrepancy when the damping is small, it is clear that a resonant absorption takes place along the entire curve, so it seems reasonable to associate the curve with some sort of surface excitation. One feature of the dips is, in fact, that they become more distinct with small damping, leading to a more pronounced nonreciprocity, in contrast to surface resonance dips in the bulk regions, which show negligible nonreciprocity for small damping [32]. In the present case, in which both the applied field and the damping are small, the dip in the upper reststrahl region is sharp, and leads to highly nonreciprocal reflectivity, but there is no visible nonreciprocity associated with the surface resonances in the bulk regions.

Figures 6(b) and 7(b) show the Goos-Hänchen shifts when damping is included. Such shifts do not significantly change from the undamped case, although the shift in the bulk regions no longer shows the symmetry observed in the undamped case [Fig. 3(c)], for which $D(B_0) = -D(-B_0)$ [20]. It is noticeable that the enhanced shifts follow the surface resonance curves in both the bulk and reststrahl regions, although, in practice, the bulk regions are of less interest because the reflectivity is essentially zero along the curves.

In the upper reststrahl region, Fig. 6(b) also includes the $\phi = 0$ solutions taken from Fig. 5(c), and there is almost exact correspondence between these results and the surface resonance curve. In fact, the $\phi = 0$ relation given by Eq. (11) is equivalent to the surface polariton relation given by Eq. (18) when the first term in the latter equation is zero, and the two equations are equal when $k_x = k_0$, corresponding to grazing incidence. Thus, when the imaginary terms of the equation dominate, as occurs here, there is little difference in the solutions.

In order to verify the enhanced Goos-Hänchen shifts for a physical incident beam, we consider the case of a Gaussian beam in Fig. 8. Here the incident beam is modeled as a plane wave sum, as in Eq. (9) with [7]

$$\psi(k_x) = -\frac{g}{2\cos\theta_i\sqrt{\pi}}\exp\left[-\frac{g^2(k_x - k_0\sin\theta_i)^2}{4\cos^2\theta_i}\right], \quad (19)$$

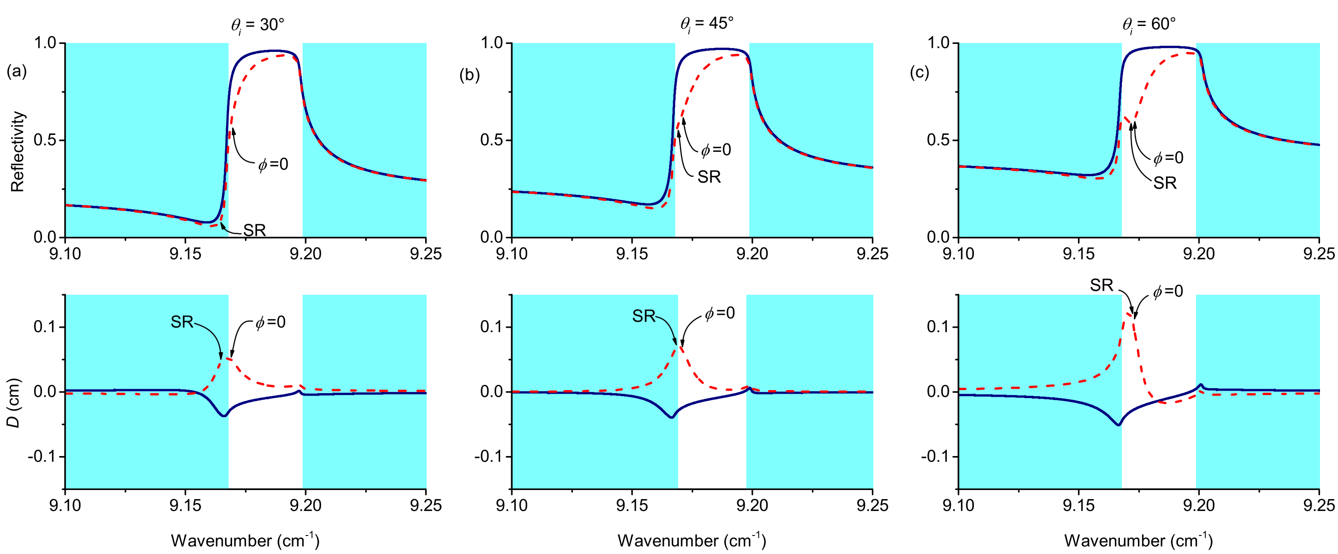

FIG. 9. Calculated reflectivity and Goos-Hänchen shift for reflection off MnF_2 in an external field B_0 of $+0.2$ T (solid blue lines) and -0.2 T (dashed red lines), at incident angles of (a) 30°, (b) 45°, and (c) 60°. The shaded regions represent the bulk regions, in which k_{2z} is real, ignoring damping. The wave-vector values marked SR are those calculated for surface resonances and those marked $\phi = 0$ are those calculated using Eq. (11) for zero damping.

where $2g$ represents the beam width in the focal plane at $z = 0$, which we take as the sample surface.

Figure 8(a) confirms that, at the surface resonance frequency, there is a negligible shift of the reflected beam for $B_0 = +0.01$ T, but a strong positive displacement, corresponding to about four free-space wavelengths, for $B_0 = -0.01$ T, in agreement with the values shown in Fig. 7(b). It is also seen that the intensity of the reflected beam when $B_0 = -0.01$ T is significantly reduced, in agreement with the reflectivity results of Fig. 7(a). Figure 8(b) shows details of the power flow near the interface, and it is seen that for $B_0 = +0.01$ T there is negligible flow into the antiferromagnet, leading to almost total reflection and negligible displacement. In the case of $B_0 = -0.01$ T, however, there is a significant penetration into the antiferromagnet, with substantial power flow along the surface, in a similar manner to that shown in Fig. 4(d) for plane waves in the absence of damping. The power flow within the antiferromagnet leads to the enhanced Goos-Hänchen shift but also results in an absorption, as seen by the diminishing intensity of the power flow along the surface. Overall, therefore, it appears that the surface resonances are characterized by significant power flow along the interface, bound to the surface, leading to a large displacement (and associated time delay) of the reflected beam, with associated absorption in the presence of damping.

V. SUMMARY AND CONCLUSIONS

We have shown how large nonreciprocal Goos-Hänchen shifts should occur on reflection off antiferromagnets in the presence of a relatively small applied magnetic field. The more significant results occur in the upper reststrahl region and show a strong link to surface resonances, which appear as extensions of the surface polariton modes that occur in this region. When damping is present, the associated power flow along the surface can lead to significant absorption, appearing as sharp dips in the reflectivity spectra.

When the applied field is larger, the effect is rather less definitive, as shown by the $B_0 = \pm 0.2$ T results in Fig. 9. The reflectivity and Goos-Hänchen shift are shown for three angles of incidence, along with the frequency values for the surface resonances and the $\phi = 0$ condition as represented by Eqs. (18) and (11), respectively. Since the two reststrahl are now well separated, we only show results around the upper reststrahl region.

All the features of interest are now closer to the bottom of the reststrahl region, with the surface resonance frequency, as calculated using Eq. (18), entering the bulk region for smaller incident angles (less than about 45° for the chosen field). This is not the case for the $\phi = 0$ result, and the two solutions are now visibly different. The corresponding reflectivity dip and the displacement peak are both somewhat broader than the separation of these two solutions, however, and the features are much less distinct, with a considerably smaller Goos-Hänchen shift than in the case of the lesser field.

Thus we can say that, at higher fields, the shifts are smaller, with less well defined features. The analysis at low fields therefore seems more productive and is likely to yield more valuable experimental results. Both the reflectivity and the beam displacement, resulting in curves of the type shown in Fig. 7, could be usefully measured to illustrate the principles. In terms of terahertz sources available for such measurements, we particularly highlight transmitters based on Schottky diode frequency multiplication of microwave oscillator signals [35]. The radiation from such transmitters can be finely tuned over the frequency range of interest and can be readily focused for experimental investigation of the phenomena of interest.

The beam displacement measurements may be somewhat prejudiced by the reduced intensity, due to absorption, of the reflected beam at the resonance frequency. There is, in general, a playoff between the resonant displacement and the reflected intensity, and this can be adjusted by varying the applied field and angle of incidence. We have, in this paper, chosen values ($B_0 = -0.01$ T, $\theta_i = 45°$) for which there is a large displacement with a reflected beam intensity that should be measurable without too much difficulty, but these values can be adjusted as necessary.

ACKNOWLEDGMENTS

The work was partially financed by the Brazilian research agencies CNPq (Grant No. 306526/2015-8) and CAPES.

[1] F. Goos and H. Hänchen, Ann. Physik **436**, 333 (1947).
[2] W. J. Wild and C. L. Giles, Phys. Rev. A **25**, 2099 (1982).
[3] O. Ivanov and D. Sementsov, Opt. Spectrosc. **89**, 737 (2000).
[4] P. T. Leung, C. W. Chen, and H.-P. Chiang, Opt. Commun. **276**, 206 (2007).
[5] R. Macêdo and T. Dumelow, J. Opt. **15**, 014013 (2013).
[6] K. Artmann, Ann. Physik **437**, 87 (1948).
[7] B. R. Horowitz and T. Tamir, J. Opt. Soc. Am. **61**, 586 (1971).
[8] M. McGuirk and C. K. Carniglia, J. Opt. Soc. Am. **67**, 103 (1977).
[9] R. H. Renard, J. Opt. Soc. Am. **54**, 1190 (1964).
[10] K. Yasumoto and Y. Ōishi, J. Appl. Phys. **54**, 2170 (1983).
[11] H. M. Lai, C. W. Kwok, Y. W. Loo, and B. Y. Xu, Phys. Rev. E **62**, 7330 (2000).
[12] W. P. Chen, G. Ritchie, and E. Burstein, Phys. Rev. Lett. **37**, 993 (1976).
[13] P. Mazur and B. Djafari-Rouhani, Phys. Rev. B **30**, 6759 (1984).
[14] S. L. Chuang, J. Opt. Soc. Am. A **3**, 593 (1986).
[15] X. Yin, L. Hesselink, Z. Liu, N. Fang, and X. Zhang, Appl. Phys. Lett. **85**, 372 (2004).
[16] H. Zhou, C. Li, and X. Che, Chin. Opt. Lett. **6**, 446 (2008).
[17] M. A. Zeller, M. Cuevas, and R. A. Depine, J. Opt. **17**, 055102 (2015).
[18] F. Lima, T. Dumelow, J. A. P. da Costa, and E. L. Albuquerque, Europhys. Lett. **83**, 17003 (2008).
[19] F. Lima, T. Dumelow, E. L. Albuquerque, and J. A. P. da Costa, Phys. Rev. B **79**, 155124 (2009).
[20] F. Lima, T. Dumelow, E. L. Albuquerque, and J. A. P. da Costa, J. Opt. Soc. Am. B **28**, 306 (2011).

[21] R. Macêdo, R. L. Stamps, and T. Dumelow, Opt. Express **22**, 28467 (2014).
[22] W. Yu, H. Sun, and L. Gao, Sci. Rep. **7**, 45866 (2017).
[23] A. S. Savchenko, A. S. Tarasenko, S. V. Tarasenko, and V. G. Shavrov, JETP Lett. **102**, 343 (2015).
[24] D. L. Mills and E. Burstein, Rep. Prog. Phys. **37**, 817 (1974).
[25] K. Abraha and D. R. Tilley, Surf. Sci. Rep. **24**, 129 (1996).
[26] T. Dumelow and M. C. Oliveros, Phys. Rev. B **55**, 994 (1997).
[27] R. E. Camley, Surf. Sci. Rep. **7**, 103 (1987).
[28] L. Remer, E. Mohler, W. Grill, and B. Lüthi, Phys. Rev. B **30**, 3277 (1984).
[29] T. Dumelow, R. E. Camley, K. Abraha, and D. R. Tilley, Phys. Rev. B **58**, 897 (1998).
[30] R. E. Camley and D. L. Mills, Phys. Rev. B **26**, 1280 (1982).
[31] R. L. Stamps and R. E. Camley, Phys. Rev. B **40**, 596 (1989).
[32] L. Remer, B. Lüthi, H. Sauer, R. Geick, and R. E. Camley, Phys. Rev. Lett. **56**, 2752 (1986).
[33] M. R. F. Jensen, S. A. Feiven, T. J. Parker, and R. E. Camley, Phys. Rev. B **55**, 2745 (1997).
[34] M. R. F. Jensen, S. A. Feiven, T. J. Parker, and R. E. Camley, J. Phys.: Condens. Matter **9**, 7233 (1997).
[35] T. W. Crowe, D. W. Porterfield, J. L. Hesler, W. L. Bishop, D. S. Kurtz, and K. Hui, Proc. SPIE **5790**, 271 (2005).